

Canuto de Almeida e Silva, Thamires and Mooste, Marek and Kibena-Pöldsepp, Elo and Matisen, Leonard and Merisalu, Mairo and Kook, Mati and Sammelseg, Väino and Tammeveski, Kaido and Wilhelm, Michaela and Rezwani, Kurosch



**Polymer-derived Co/Ni-SiOC(N) ceramic electrocatalysts for oxygen reduction reaction in fuel cells**

Journal Article as: peer-reviewed accepted version (Postprint)

DOI of this document\* (secondary publication): <https://doi.org/10.26092/elib/2490>

Publication date of this document: 26/09/2023

\* for better findability or for reliable citation

**Recommended Citation (primary publication/Version of Record) incl. DOI:**

Canuto de Almeida e Silva, Thamires and Mooste, Marek and Kibena-Pöldsepp, Elo and Matisen, Leonard and Merisalu, Mairo and Kook, Mati and Sammelseg, Väino and Tammeveski, Kaido and Wilhelm, Michaela and Rezwani, Kurosch,  
Polymer-derived Co/Ni-SiOC(N) ceramic electrocatalysts for oxygen reduction reaction in fuel cells,  
Catal. Sci. Technol., 2019, 9, 3, 854-866, The Royal Society of Chemistry  
<https://doi.org/10.1039/C8CY02207K>

Please note that the version of this document may differ from the final published version (Version of Record/primary publication) in terms of copy-editing, pagination, publication date and DOI. Please cite the version that you actually used. Before citing, you are also advised to check the publisher's website for any subsequent corrections or retractions (see also <https://retractionwatch.com/>).

This document is made available with all rights reserved.

**Take down policy**

If you believe that this document or any material on this site infringes copyright, please contact [publizieren@suub.uni-bremen.de](mailto:publizieren@suub.uni-bremen.de) with full details and we will remove access to the material.

# Polymer-derived Co/Ni–SiOC(N) ceramic electrocatalysts for oxygen reduction reaction in fuel cells†

Thamires Canuto de Almeida e Silva,<sup>a</sup> Marek Mooste,<sup>b</sup> Elo Kibena-Põldsepp,<sup>b</sup> Leonard Matisen,<sup>c</sup> Mairo Merisalu,<sup>bc</sup> Mati Kook,<sup>c</sup> Väino Sammelselg,<sup>bc</sup> Kaido Tammeveski,<sup>id \*b</sup> Michaela Wilhelm<sup>id \*a</sup> and Kurosch Rezwani<sup>id ad</sup>

Cobalt/nickel-containing SiOC-based porous ceramic electrocatalysts were prepared by pyrolysis of poly(methyl silsesquioxane) and poly(methyl phenyl silsesquioxane) as preceramic precursors combined with graphite and Co/Ni metal salts at 1000 °C in an atmosphere of nitrogen. Subsequently, the Co/Ni–SiOC materials were N-doped using dicyandiamide (DCDA) as a nitrogen source and pyrolysed at 800 °C in an inert atmosphere. The structural properties and composition of the catalysts were characterised by scanning electron microscopy (SEM), X-ray diffraction, X-ray photoelectron spectroscopy (XPS) and N<sub>2</sub> adsorption analysis. The evaluation of the polymer-derived SiOC(N) ceramic electrocatalysts as a new class of catalysts for the oxygen reaction reduction (ORR) was carried out by the rotating disk electrode (RDE) method under acidic, neutral and alkaline conditions. The O<sub>2</sub> reduction studies revealed that the N-doped materials exhibited enhanced ORR performance, confirming the positive influence of the nitrogen functionalities introduced into the catalysts. The Co-containing N-doped SiOC catalyst exhibited significantly higher ORR activity compared with the studied materials along with the highest electron transfer number in all the studied solutions. Long-term ORR performance testing indicated that the durability of this catalyst was superior as compared to that of commercial Pt/C. These observations suggest that the Co-containing N-doped SiOC catalyst is a promising cathode material for fuel cells (FCs) and microbial FC devices.

Received 25th October 2018,  
Accepted 7th January 2019

DOI: 10.1039/c8cy02207k

## 1. Introduction

The increased demand for energy sources and global warming have required great efforts regarding the development and optimisation of renewable energy devices. Among the available technologies, fuel cells (FCs) are promising energy conversion devices due to their high power density, easy deployment in different areas and weather conditions, and low maintenance costs.<sup>1,2</sup> Extending the environmental needs to water treatment, microbial fuel cells (MFCs) also play an important role as a self-sustaining technology, which converts chemical energy from biodegradable substrates, *e.g.* effluents, into electrical energy *via* an active biocatalyst.<sup>3,4</sup> The oxygen reduction

reaction (ORR), which takes place at the cathode in FC and MFC devices, frequently limits the performance as a result of its slow reaction kinetics.<sup>2</sup> Furthermore, the electrode potential and pH value of the electrolyte solution also influence the ORR pathway and mechanism.<sup>5,6</sup> This is particularly true under neutral operating conditions of MFCs, where a low concentration of supporting electrolytes and room temperature lower the ORR performance.<sup>5,7</sup> The ORR is a multi-step reaction, where oxygen can be directly reduced to water *via* a 4e<sup>-</sup> pathway or a two-step 2e<sup>-</sup> pathway, forming hydrogen peroxide as an intermediate product.<sup>2,8</sup> Suitable electrocatalysts should support either the 4e<sup>-</sup> or 2 × 2e<sup>-</sup> pathway with minimal production of hydrogen peroxide, to avoid degradation of fuel cell components and restricted efficiency.<sup>8</sup> Therefore, many approaches have focused on developing stable and cost-effective catalysts with enhanced electrocatalytic activity in the interest of improving the FC performance. Platinum is the best catalyst and carbon-supported Pt (Pt/C) is the state-of-the-art material due to its high activity towards the ORR under acidic and alkaline conditions.<sup>9</sup> However, the high costs, limited availability and long-term stability issues of Pt-sources limit the commercial viability of low-temperature fuel cells, which operate generally with Pt-based

<sup>a</sup> University of Bremen, Advanced Ceramics, Am Biologischen Garten 2, JW3, 28359, Bremen, Germany. E-mail: m.wilhelm@uni-bremen.de; Fax: +49 421 218 64932; Tel: +49 421 218 64944

<sup>b</sup> Institute of Chemistry, University of Tartu, Ravila 14a, 50411 Tartu, Estonia. E-mail: kaido.tammeveski@ut.ee; Fax: +372 7375181; Tel: +372 7375168

<sup>c</sup> Institute of Physics, University of Tartu, W. Ostwald Str. 1, 50411 Tartu, Estonia

<sup>d</sup> MAPEX Center for Materials and Processes, University of Bremen, 28359, Bremen, Germany

† Electronic supplementary information (ESI) available: Figures and tables. See DOI: 10.1039/c8cy02207k

electrocatalysts.<sup>8,10,11</sup> Proposed alternatives to ORR electrocatalysts to address Pt-based material issues can be divided into carbon-based, transition metal-containing and/or nitrogen-doped carbon (M–N–C or N–C) materials.<sup>12–14</sup>

Many different high surface area carbon-based nanomaterials have already been studied as ORR catalysts for fuel cell applications.<sup>8,15,16</sup> In spite of the high surface area of carbon-based materials, usually the electrocatalytic activity of pristine carbon nanomaterials towards the ORR is quite modest.<sup>8,17,18</sup> Therefore, N–C or M–N–C catalysts hold the most promising results to replace Pt under alkaline conditions.<sup>8,14</sup> In order to enhance the electrocatalytic properties of nanocarbons, functionalisation of these materials with nitrogen and transition metal (*e.g.* Co) through high-temperature treatment in an inert atmosphere (*i.e.* pyrolysis)<sup>8,16</sup> has been conducted. The rise in the ORR activity due to co-doping with Co and N *via* pyrolysis has been proven to be effective on different carbon materials such as carbon nanotubes (CNTs),<sup>19–23</sup> carbon aerogels,<sup>24–26</sup> graphene,<sup>27,28</sup> carbon spheres,<sup>29</sup> carbon nanocomposites,<sup>30–33</sup> porous carbon,<sup>34–38</sup> carbon nanofibers,<sup>39–43</sup> carbon dots,<sup>44</sup> and carbon black.<sup>45</sup> As a cheap and effective reagent, dicyandiamide (DCDA) has often been used as a nitrogen precursor for the functionalisation of carbon materials with nitrogen during pyrolysis.<sup>20,22,23,25,28,32,36,38,45–48</sup> Even though carbon-based materials possess features such as easy processability, a wide potential window, sufficient electrical conductivity, and low costs when used as catalyst supports, their low resistance to corrosion is currently a technical barrier.<sup>1,49,50</sup>

Silicon oxycarbide (SiOC) is an interesting type of polymer-derived ceramic (PDC) since its properties can be tailored by varying the starting preceramic polymers and pyrolysis conditions. SiOC-based ceramics possess high chemical and thermal stability, semiconducting behaviour and allow the adjustment of surface properties. The high stability of SiOC is a result of the amorphous structure made of SiO<sub>2</sub>/C nanodomains whereas the existing conduction paths are related to its disordered carbon structure.<sup>51,52</sup> These functional properties can additionally be modified by incorporation of fillers into the SiOC matrix, such as Mo, Si, Ti, MoSi<sub>2</sub> and SiC to improve the stability and mechanical properties.<sup>53</sup> Besides, when metal sources such as metal oxides and metal salts are used, their *in situ* reduction during pyrolysis results in metal nanoparticles embedded in a SiOC support.<sup>54–57</sup> Due to its stability, tunable properties and simple preparation routes with the feasibility of *in situ* formation of metal nanoparticles, SiOC has been investigated as a metal-containing PDC catalyst in the CO oxidation reaction and as an electrocatalyst under acidic conditions (0.1 M H<sub>2</sub>SO<sub>4</sub>),<sup>54,58</sup> in isopropyl alcohol conversion,<sup>59</sup> CO<sub>2</sub> methanation and Fischer-Tropsch reaction,<sup>60</sup> but the ORR has not so far been investigated. The obtained catalytic activity in these studies has been related to thermal stability, metal distribution, cross-linking densities and accessibility of the catalytic sites, as well as the degree of surface hydrophilicity of the SiOC-based materials developed, respectively. On the other hand, few studies have focused on N-doped SiO

In this work, we developed polymer-derived SiOC(N) ceramic electrocatalysts and investigated their applicability as a new class of catalysts for the ORR. The synthesis included nitrogen doping of SiOC-based materials by pyrolysis with DCDA, which has not been reported in the context of ORR catalyst synthesis. The ORR activity of the catalysts was evaluated under acidic, neutral, and alkaline conditions. The findings can contribute to the fundamental understanding related to the change in activity as a result of pH conditions, and can be used to define the applicability of these novel materials to a variety of low-temperature fuel cells.

## 2. Experimental section

### 2.1 Preparation of polymer-derived SiOC(N) electrocatalysts and electrodes

**2.1.1 Material preparation.** The polymer-derived ceramic (PDC) based materials were synthesised according to an adapted procedure used for conductive porous materials as well as hybrid materials containing metallic nanoparticles reported previously.<sup>62,63</sup> Briefly, silicon resin poly(methyl silsesquioxane) (MK, Wacker Chemie AG) and poly(methyl phenyl silsesquioxane) (H44, Wacker Chemie AG) were used as preceramic precursors combined with graphite (KS75, IMERYL Graphite & Carbon) as a carbon source for a minimal electrical conductivity. Additional fillers, such as molybdenum disilicide (MoSi<sub>2</sub>, aber GmbH) and azodicarboxamide (Azo, Sigma-Aldrich Co), were used for shrinkage control related to the polymer-to-ceramic conversion and pore formation, respectively. For the Co/Ni-containing materials, metal salts such as nickel chloride (NiCl<sub>2</sub>, Alfa Aesar) and cobalt chloride (CoCl<sub>2</sub>, Alfa Aesar) were used as precursors for metal nanoparticle formation. The powder materials were dissolved/dispersed under constant stirring at room temperature using xylene (Sigma-Aldrich) as a solvent. A cross-linking step was initiated by the addition of the catalyst imidazole (Imi, Alfa Aesar) and stirring for 20 min. The mixture of reagents was then dried and the resultant materials were subjected to pyrolysis under a N<sub>2</sub> atmosphere. The heating up was performed with 120 K h<sup>-1</sup> up to 900 °C and with 30 K h<sup>-1</sup> up to 1000 °C, with a dwelling time of 4 h. With a cooling rate of 120 K h<sup>-1</sup>, the pyrolysis ended. The pyrolysed materials were ground and sieved to particle sizes <300 μm. The resulting powders were further ball-milled (PM 400, Retsch) at 350 rpm min<sup>-1</sup> for 4 h to produce a fine powder. The obtained samples are denoted as PDC, PDC-Ni, and PDC-Co and their compositions are presented in Table S1 in the ESI.†

PDC, PDC-Ni and PDC-Co were doped with nitrogen using a previously optimised procedure.<sup>48</sup> As the nitrogen source, dicyandiamide (DCDA) was added in a weight ratio of 1:20 (DCDA:PDC, PDC-Ni or PDC-Co). Polyvinylpyrrolidone was used as a surface-active agent, in an amount of 1/10 of the corresponding PDC material. The mixture of reagents was transferred to a beaker containing 2-propanol (99.8%, Honeywell Riedel-de Haën) and sonicated for 2 h to achieve a homogeneous mixture. Subsequently, 2-propanol was

evaporated in a vacuum at 60 °C. The material was collected in a quartz boat and pyrolysed in a flowing N<sub>2</sub> atmosphere at 800 °C for 2 h using a heating rate of 10 °C min<sup>-1</sup>. After pyrolysis, the furnace was slowly cooled to room temperature and the products were collected and weighed. The N-doped catalyst materials are marked with additional -N in the designation: PDC-N, PDC-Ni-N, PDC-Co-N.

**2.1.2 Electrode preparation.** For the electrochemical experiments, a glassy carbon (GC) electrode with a geometric area (A) of 0.196 cm<sup>2</sup> was used as an underlying substrate. The electrode was prepared by mounting the GC disc (GC-20SS, Tokai Carbon, Japan) into a Teflon® holder and then the GC electrode surface was polished before use with 1.0 and 0.3 μm alumina slurries (Buehler). The surface of the GC electrode was cleaned by sonication in Milli-Q water (Millipore, Inc.) and 2-propanol for 5 min in each solvent. For coating the GC electrode with the catalyst materials, 2 mg of the corresponding nanomaterial were dispersed in 1 mL of 2-propanol, followed by sonication for 1 h. After the sonication, 10 × 2 μL of the catalyst ink was pipetted onto the polished GC surface. After solvent evaporation in air, 0.2 mg cm<sup>-2</sup> catalyst loading was obtained. Prior to electrochemical measurements, the electrodes were carefully rinsed with Milli-Q water. For clarification, the catalyst-coated GC electrodes are designated as the underlying material (GC) followed by the catalyst material.

For comparison purposes, the Pt/C catalyst coated GC electrode was also used. The commercial 20 wt% Pt catalyst supported on Vulcan carbon XC-72 was acquired from E-TEK, Inc. (Framingham, MA, USA) and dispersed in 2-propanol. The GC electrode was coated with Pt/C ink in a similar manner to the other studied nanomaterials, resulting in a Pt loading of 40 μg cm<sup>-2</sup>.

## 2.2 Material characterisation

**2.2.1 BET, XRD, SEM, TEM, XPS and electrical conductivity measurements.** The specific surface area (SSA) of the catalysts was determined using nitrogen adsorption-desorption isotherms measured at 77 K using the Belsorp-Mini equipment (Bel Japan, Inc.) and calculated by the BET (Brunauer, Emmett, and Teller) method. The materials were pretreated at 120 °C for 3 h under vacuum. The phase structure of the PDC-based materials was identified by X-ray diffraction (XRD) on an Iso-Debyeflex SEIFERT diffractometer that uses a Bragg-Brentano geometry and Cu-Kα radiation with a wavelength of 0.154 nm at 40 kV and 40 mA. Data were recorded from 5 to 80° in 0.025° steps. For the N-doped materials, an additional XRD system (Bruker D8 Advance diffractometer) with Ni filtered Cu-Kα radiation, 0.6 mm (0.3°) wide parallel beam, two 2.5° Soller slits, and a LynxEye line detector was used. Data were recorded from 21 to 80° in 0.0149° steps. The microstructure and metal nanoparticles were analysed by scanning electron microscopy (SEM). For the SEM experiments, a high-resolution scanning electron microscope (HR-SEM) (Helios NanoLab 600 (FEI Company)) equipped with an

energy-dispersive X-ray (EDX) spectrometer analyser (INCA Energy 350 (Oxford Instruments)) and a field emission SEM (SUPRA 40-Carl (Zeiss, Germany)) equipped with an EDX XFlash 6|30 detector (Bruker) were used. Transmission electron microscopy (TEM) measurements were carried out on an imaging Cs-corrected TITAN 80/300 (FEI) machine operating at 300 kV.

For the X-ray photoelectron spectroscopy (XPS) measurements, 11 × 11 mm<sup>2</sup> plates of GC were coated with nanomaterials. The spectra were acquired with a SES-100 spectrometer at 200 eV pass energy. Survey spectra were acquired with 500 meV steps and core-level spectra with 100 meV steps. The excitation source used was a non-monochromatic Thermo XR3E2 dual anode X-ray gun. Mg (Kα at 1253.6 eV) at 300 W was used for PDC-Ni and Al (Kα at 1486.6 eV) at 400 W was used for all the other samples. The vacuum in the analysis chamber was below 10<sup>-9</sup> torr at all times. The N1s XPS peak was deconvoluted into 5 components:<sup>64,65</sup> (i) pyridinic-N, (ii) amines/M-N<sub>x</sub>, (iii) pyrrolic-N, (iv) graphitic-N, and (v) pyridine-N-oxides. The peak binding energy positions were found to be: (i) 398.0 eV, (ii) 399.2 eV, (iii) 400.7 eV, (iv) 402.7 eV and (v) 404.5 eV. The FWHM was constrained from 1 eV to 2 eV for peaks (i)-(iv) and 1 eV to 2.5 eV for peak (v). Peak positions were constrained: (i) 398.1-397.7 eV, (ii) 399.7-399.1 eV, (iii) 401.7-400.5 eV, (iv) 403-402.6 eV and (v) 403.8-405.8 eV. All peaks were assumed to be 70% Gaussian and 30% Lorentzian. A linear background was used for only PDC-Co; for all other peaks Shirley background was used. The software CasaXPS (2.3.18) was used for peak fitting.

Measurements of electrical conductivity were carried out according to Moni *et al.*<sup>66</sup> Briefly, the materials were pressed into a pellet and placed between stainless steel blocking electrodes connected with an impedance analyzer (Impedance Measurement Unit IM6ex Zahner Electric). The measurements were performed in the frequency range of 1 MHz to 10 mHz with an AC amplitude of 10 mV at 25 °C.

## 2.3 Electrochemical measurements

The electrochemical measurements were carried out in an Ar-saturated (99.999%, AGA) or O<sub>2</sub>-saturated (99.999%, AGA) aqueous solution using cyclic voltammetry (CV), linear sweep voltammetry (LSV) and rotating disc electrode (RDE) methods. Three different electrolyte solutions were used: i) 0.1 M KOH (p.a. quality, Merck), ii) 0.1 M phosphate buffer solution (PBS) (pH = 7) containing 0.1 M NaClO<sub>4</sub> (pro analysi, Merck) and iii) 0.5 M H<sub>2</sub>SO<sub>4</sub> (96% Suprapur®, Merck). The buffer solution was prepared from Na<sub>2</sub>HPO<sub>4</sub> (puriss p.a., Fluka) and KH<sub>2</sub>PO<sub>4</sub> (pro analysi, Merck). The electrochemical experiments were performed with an Autolab potentiostat/galvanostat PGSTAT128N (Metrohm Autolab, The Netherlands) controlled with Nova 2.1 software. A three-compartment electrochemical cell with Pt wire as a counter electrode and a saturated calomel electrode (SCE) as a reference electrode was used. For the RDE measurements, an EDI101 rotator and a CTV101 speed control unit

(Radiometer) were employed. The following electrode rotation rates ( $\omega$ ) were used for RDE experiments: 360, 610, 960, 1900, 3100 and 4600 rpm. All the presented RDE polarisation curves are recorded in the cathodic direction. All the potentials mentioned in this study are referenced to the reversible hydrogen electrode (RHE). For the conversion of potential values from *vs.* SCE to *vs.* RHE, the following equation  $E_{\text{RHE}} = E_{\text{SCE}} + 0.241 \text{ V} + 0.059 \times \text{pH}$  was used.

### 3. Results and discussion

#### 3.1 Physical characterisation of SiOC(N)-based electrocatalysts

Fig. 1 summarises the SEM micrographs (50 000 $\times$  magnification) of the different SiOC materials tested in this work. Ball-milling is used to grind the ceramic material in order to reduce the particle size of the material and the SEM results show that ball-milling for 4 h at 350 rpm refined the SiOC ceramic material into powder with particle sizes smaller than 20  $\mu\text{m}$  (see Fig. 1a). The doping of the materials with Ni, Co and N has no visible effect on the structure of the SiOC powder (see Fig. 1b–f) as expected. The SEM micrographs with 5000 $\times$  magnification are presented in Fig. S1 in the ESI $\dagger$  for comparison.

Nitrogen adsorption–desorption measurements were performed in order to characterise the porosity and BET SSA of the PDC-based materials (Fig. 2). According to the IUPAC classification, all the materials reveal type IV isotherms with a hysteresis loop close in shape to a type H3, indicating the

presence of mesopores (pore diameter 2–50 nm).<sup>67</sup> The type H3 loop is often linked with plate-like particles or slit-shaped pores,<sup>68,69</sup> which was also supported by the SEM images (Fig. 1). The presence of mesopores enhances mass transport and access of active sites and is thus essential for the ORR performance. The size distribution of mesopores obtained by the Barrett–Joyner–Halenda (BJH) method is shown in the insets of Fig. 2 and S2. $\dagger$  Table S2 $\dagger$  summarises the pore characteristics of the PDC materials. The materials exhibit a broad pore size distribution (Fig. 2 and S2 $\dagger$ ) and an increase in pore volume and pore size (Table S2 $\dagger$ ) for the N-doped catalysts compared to the pristine materials. The SSA values for the pristine materials are in the range of 6–8  $\text{m}^2 \text{g}^{-1}$  and are attributed to the rather high pyrolysis temperature of 1000  $^\circ\text{C}$ , at which the collapse of micropores occurs during the polymer-to-ceramic conversion.<sup>70</sup> A slight increase in SSA is observed for the Co-containing material. The SSA increases significantly for the N-doped materials and could offer more adsorption and reactive sites, influencing the enhancement of electrocatalytic activity.

Fig. 3 shows the XRD patterns of the studied Ni/Co-containing pristine and N-doped PDC electrocatalyst materials. After pyrolysis at 1000  $^\circ\text{C}$ , polysiloxane derived ceramics are normally amorphous SiOC.<sup>71</sup> The diffraction patterns of all the materials reflect similar main peaks. The identified peaks at ( $2\theta$ ) 22.6 $^\circ$ , 30.1 $^\circ$ , 39.7 $^\circ$ , 44.6 $^\circ$ , 46.2 $^\circ$ , 57.4 $^\circ$ , 62.5 $^\circ$ , 66.2 $^\circ$ , 72.2 $^\circ$ , 75.5 $^\circ$ , 76.7 $^\circ$ , and 85.6 $^\circ$  are attributed to the filler molybdenum disilicide (PDF 041-0612) and the peaks at 26.5 $^\circ$ , 42.4 $^\circ$ , 44.6 $^\circ$ , 54.6 $^\circ$ , 77.5 $^\circ$ , and 83.7 $^\circ$  to carbon (graphite)

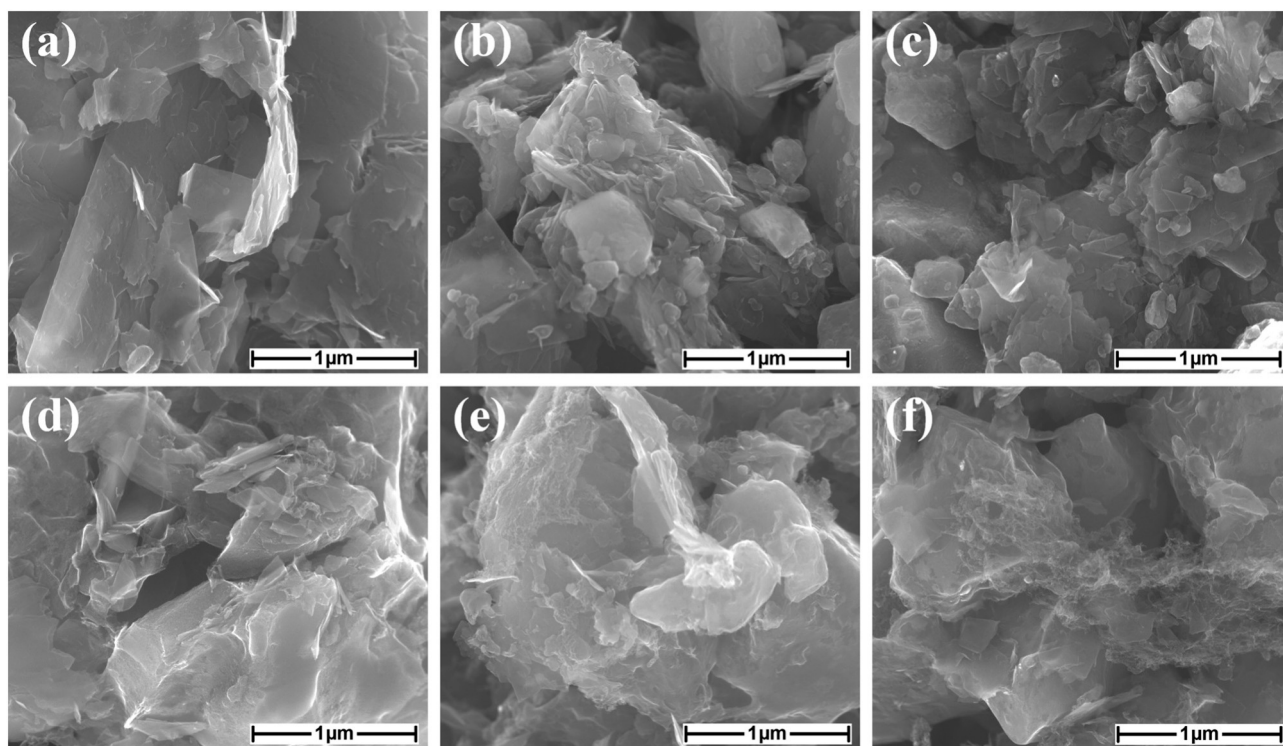


Fig. 1 SEM images (50 000 $\times$  magnification, scale bar: 1  $\mu\text{m}$ ) of (a) PDC, (b) PDC-Ni, (c) PDC-Co, (d) PDC-N, (e) PDC-Ni-N, and (f) PDC-Co-N catalyst materials on the glassy carbon electrode.

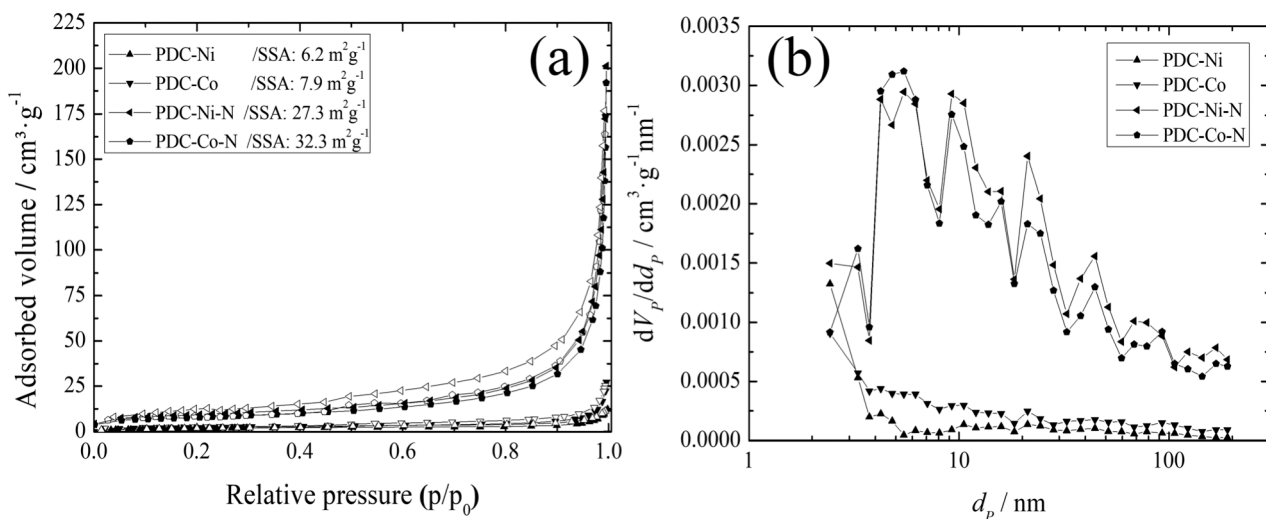


Fig. 2 Nitrogen adsorption-desorption isotherms, respective specific surface areas (a), and Barrett-Joyner-Halenda (BJH) pore size distribution plot (b) of the PDC-Ni, PDC-Co, PDC-Ni-N and PDC-Co-N materials.

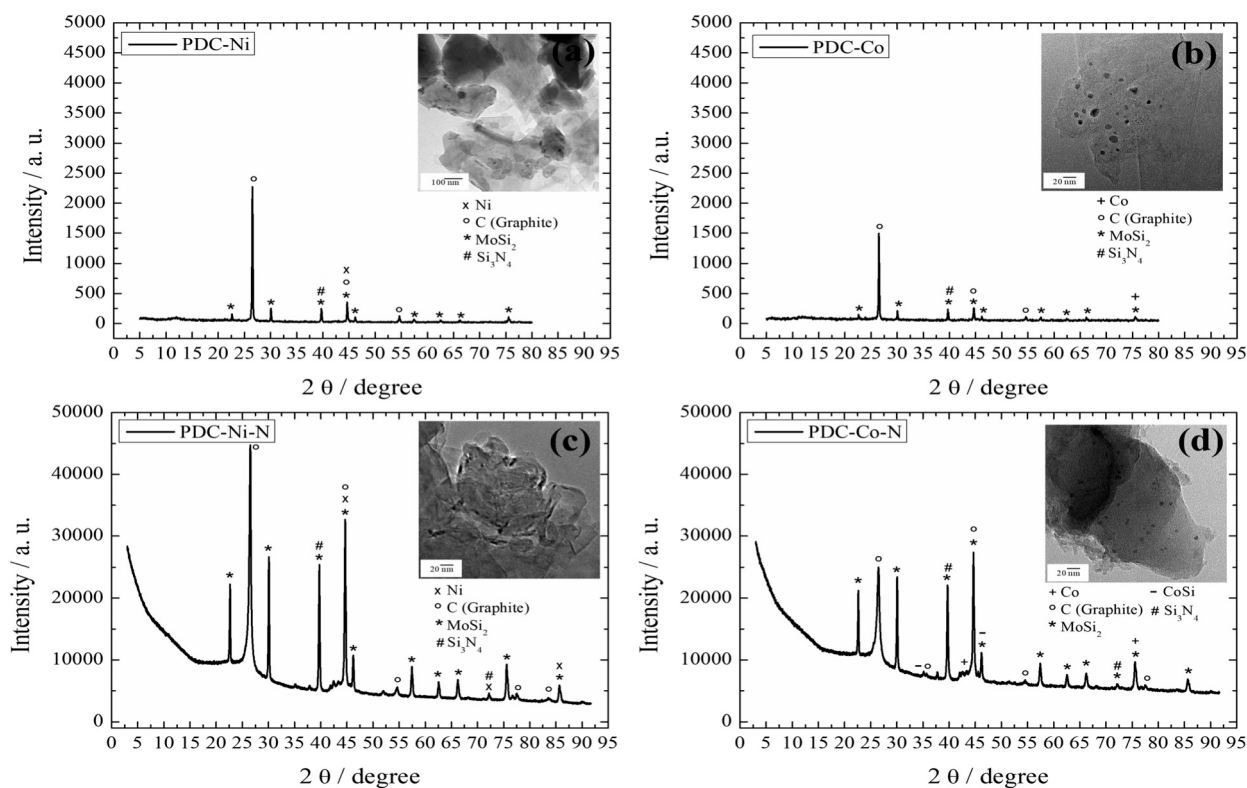


Fig. 3 XRD patterns of the PDC-Ni (a), PDC-Co (b), PDC-Ni-N (c) and PDC-Co-N (d) materials and their respective TEM images (insets).

2H, PDF 01-089-7213) with preserved crystalline phases after pyrolysis. Furthermore, the peaks at  $2\theta$ , 39.7°, 41.8°, 45.6°, and 85.5° and those at 44.6°, 51.4°, and 75.8° refer to a small amount of metallic Ni (PDF 01-089-7129) and Co (PDF 01-089-4307), respectively. In addition, the peaks at 39.7° and 72.1° evidence the initial crystallisation of silicon nitride Si<sub>3</sub>N<sub>4</sub> (PDF 00-005-0659) and those at 45.6° of cobalt silicide CoSi, as a product of the reaction between Co particles and the SiOC matrix (PDF 03-065-3296). The TEM images of the

Ni or Co-containing materials are shown in the insets of Fig. 3. The Ni and Co metallic particles could be observed and present different sizes varying from 7 to 40 nm for Ni and from 2 to 14 nm for Co. For the N-doped materials, smaller particles were visualised with mean values of about 5 nm.

The electrical conductivity values of the PDC-based materials measured at room temperature are additionally shown in Table S2.† The values vary from 0.03 to 0.09 S cm<sup>-1</sup>

suggesting a semiconductor behaviour.<sup>71</sup> A decrease in conductivity is found for the N-doped materials and can be correlated with the increased pore size and increased porosity which tends to lower the electrical conductivity in accordance with previous observations.<sup>72</sup>

Fig. 4 presents the XPS survey spectra of the studied materials. In all cases, the XPS peaks of O1s, C1s, Si2s, and Si2p corresponding to O, C and Si can be observed, as expected for SiOC-based materials.<sup>73</sup> The detection of nitrogen (N1s) further confirmed the successful N-doping of the PDC-based

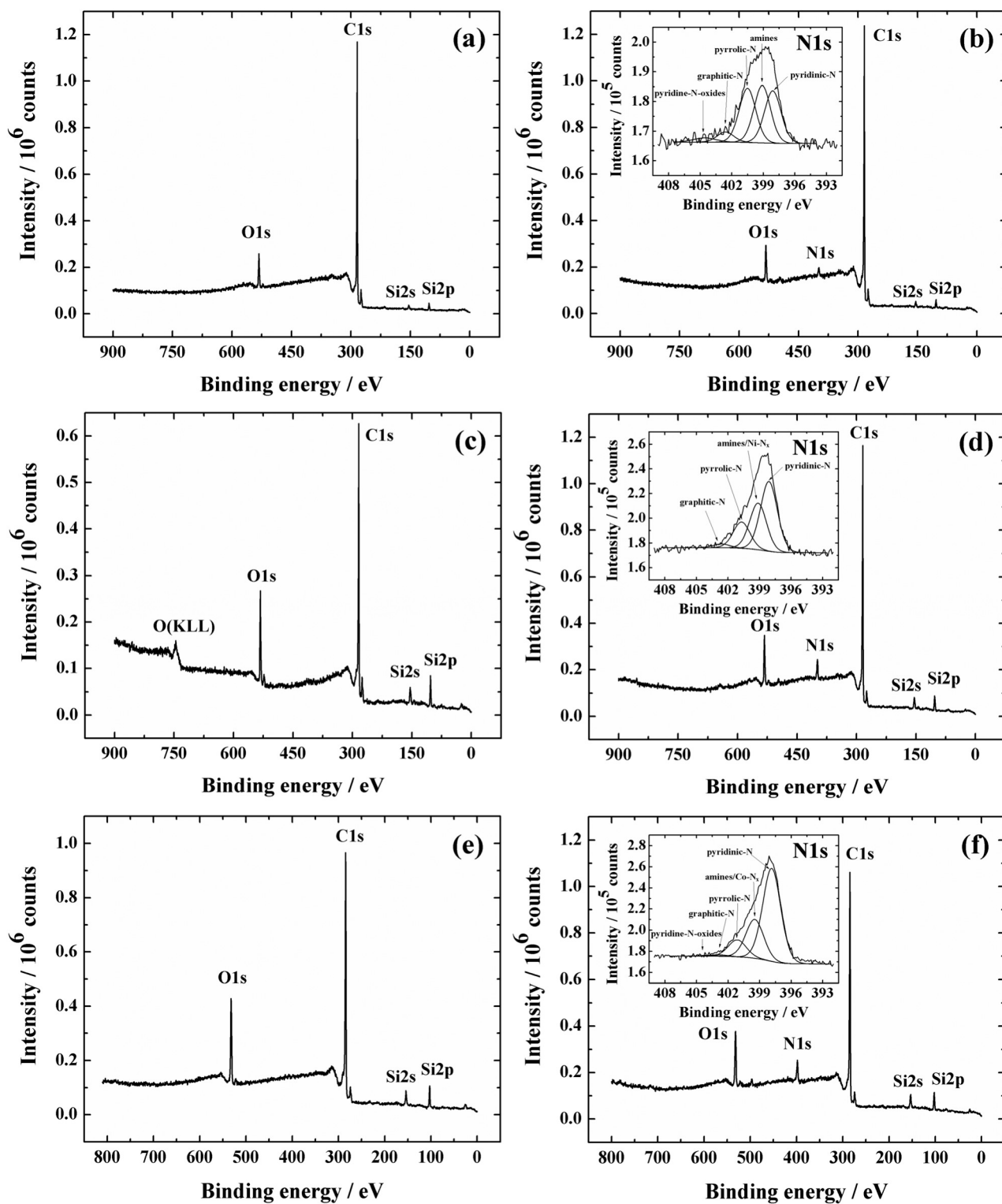


Fig. 4 XPS survey spectra of (a) PDC, (b) PDC-N, (c) PDC-Ni, (d) PDC-Ni-N, (e) PDC-Co, and (f) PDC-Co-N catalyst materials on the glassy carbon electrode. The insets in b, d, and f show the high-resolution XPS spectra in the N1s region.

catalysts. However, the intensity of the XPS peaks for Co and Ni (Fig. 4c–f) is so low that these are rather difficult to distinguish in the XPS wide scan spectra. This is a relatively common phenomenon and has been previously observed in studies on carbon nanomaterial based ORR catalysts with low Co loading.<sup>31,39,46</sup> In the present work, the content of transition metals (Co or Ni) resulting from the thermal decomposition of cobalt(II) and nickel(II) chloride was calculated to be less than 3 wt% in the PDC matrix. The contents of different elements in the catalyst materials calculated from the high-resolution XPS spectra and SEM–EDX data are presented in Table S3.† According to the SEM–EDX data, the chemical composition of the ceramic catalysts does not significantly vary, presenting *ca.* 7 at% Si, 20 at% O and 68 at% C as a result of the polysiloxane conversion into ceramics and an additional amount of the carbon source used. The nitrogen content (*ca.* 2 at%) present on the pristine materials corresponds to the residual amount of the pore-forming agent azodicarbonyl amide, due to incomplete decomposition after heat treatment at 1000 °C (data not shown). Furthermore, the increase in the nitrogen content to *ca.* 6 at% was observed for all the N-doped materials, confirming successful doping using DCDA. Regarding Co/Ni, a content of *ca.* 0.3 at% was observed for all the transition metal-containing catalyst materials (see Table S3.†). The C1s, O1s and Si2p representative core-level XPS spectra of the PDC-Co and PDC-Co–N materials are also presented in Fig. S3.† The main C-signal identified in C1s can be attributed to the free carbon (284 eV).<sup>73</sup> Low intensity C-signals from 286 to 289 eV correspond to carbon oxygenated groups or C–N and those at 283 eV to C–Si bonds.<sup>73,74</sup> The O1s spectra reveal a broad peak with a peak energy of about 533 eV indicating the presence of Si–O bonds and a low intensity peak at 536 eV typical of C–O bonds.<sup>75</sup> The Si2p spectra exhibit signals from 102 to 103 eV, corresponding to Si–O–C bonds and the Si–O bond, respectively.<sup>76</sup> It is possible that these signals also mask the Si–C and Si–N signals, due to the high % of SiOC and SiO<sub>2</sub> in the Si2p spectra. The core-level XPS spectra collected in the Co2p region for PDC-Co and PDC-Co–N catalysts are shown in Fig. S4.† The clear difference between these two XPS spectra is the considerably higher amount of Co photoelectrons recorded at *ca.* 781 eV in the case of PDC-Co–N compared to PDC-Co. According to the literature,<sup>37,38,42,46,47</sup> the corresponding peak at *ca.* 781–782 eV conforms to Co–N<sub>x</sub>, which indicates that a considerable amount of Co could be coordinated to nitrogen in the case of PDC-Co–N compared to the material that has not been pyrolysed in the presence of the nitrogen source (PDC-Co).

The deconvoluted N1s XPS spectra of the nitrogen-doped catalysts are presented in the insets of Fig. 4b, d and f and the relative content (%) of different nitrogen species is given in Table 1.

In the case of the PDC–N material, the content of pyridinic-N, amines and pyrrolic-N is very similar (around 30%). The N1s peak of amines could also correspond to the nitrile groups because of the possible disappearance of amine groups during high-temperature heat-treatment.<sup>25</sup> Likewise, the N1s peaks of pyridinic-N could also be assigned to N–Si bonds.<sup>61,77</sup> In the case of both transition metal (Co and Ni) and nitrogen co-doped catalysts, the suppression of the pyridine-N-oxide peak has also been noticed in our previous work with carbon aerogel-based catalysts.<sup>25</sup> In the comparison of PDC–Ni–N with the PDC–N material, the relative decrease in pyrrolic-N and increase in pyridinic-N are pronounced. A very similar tendency has been observed for pyrolysed N-doped carbon and nickel nitride composite materials and this could correspond to the conversion of the nitrogen species among each other during pyrolysis.<sup>78</sup> PDC–Co–N is the catalyst with the highest N content (7 at%) studied in the present work (see Table S3.†). According to the literature, Co could act as a booster for increasing nitrogen content by creating more nitrogen moieties that are electrocatalytically active towards the ORR from initial nitrogen sources.<sup>79</sup> This could be the explanation for the highest total content of N, lower content of pyrrolic-N and higher content of pyridinic-N in PDC–Co–N compared to those in the PDC–Ni–N catalyst (see Table 1). In addition to pyridinic-N, Co–N<sub>x</sub> contributes at a very similar binding energy value of *ca.* 399 eV to the N1s XPS spectra.<sup>47</sup> Also, the presence of Co–N<sub>x</sub> species<sup>45,47</sup> is most likely detected in the Co2p region (see Fig. S4.†).

### 3.2 ORR studies in alkaline, neutral and acid media

**3.2.1 Cyclic voltammetry and linear sweep voltammetry studies.** The electrochemical behaviour of the catalyst materials was studied in three different aqueous solutions: i) 0.1 M KOH (pH = 13), ii) 0.1 M PBS containing 0.1 M NaClO<sub>4</sub> (pH = 7), and iii) 0.5 M H<sub>2</sub>SO<sub>4</sub> (pH = 0.3). Fig. S5.† presents the cyclic voltammograms (CVs) of the bare and nanomaterial-coated GC electrodes recorded in Ar-saturated electrolyte solutions. The electrodes were cycled until a reproducible CV was obtained. The baseline current density in the studied potential range for all the catalyst material coated GC electrodes is significantly higher compared to that of the bare GC electrode. This is a typical CV behaviour of electrodes coated with high-area electrochemically active

**Table 1** Relative content (%) of different nitrogen species determined for the N-functionalised catalyst materials from deconvoluted N1s XPS peaks shown in Fig. 4b, d and f

Catalyst material	Pyridinic-N	Amines/Me–N <sub>x</sub>	Pyrrolic-N	Graphitic-N	Pyridine-N-oxide
PDC–N	29	32	30	6	3
PDC–Ni–N	48	32	18	3	—
PDC–Co–N	61	26	11	1	1

carbon nanomaterials (e.g. graphene, multi-walled carbon nanotubes) due to the higher electrical double layer capacitance compared to the polished GC electrode.<sup>80,81</sup>

In Fig. S6,<sup>†</sup> the linear sweep voltammograms (LSVs) of the studied electrodes in O<sub>2</sub>-saturated solutions are presented in an analogous layout to CVs in Fig. S5.<sup>†</sup> In all the solutions,

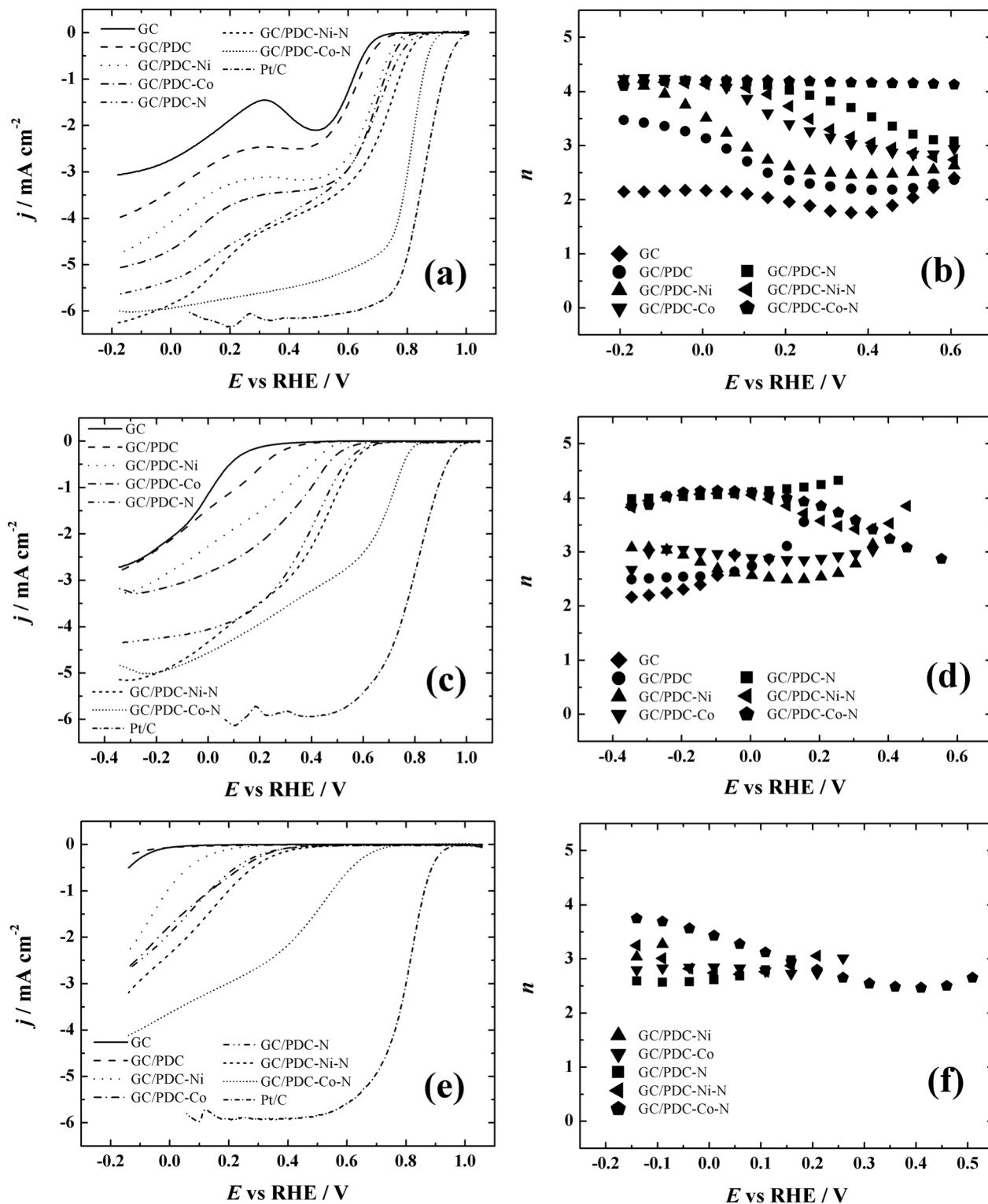


Fig. 5 RDE voltammetry curves for O<sub>2</sub> reduction on different electrodes in O<sub>2</sub>-saturated 0.1 M KOH (pH = 13) (a), 0.1 M PBS containing 0.1 M NaClO<sub>4</sub> (pH = 7) (c) and 0.5 M H<sub>2</sub>SO<sub>4</sub> (pH = 0.3) (e) ( $\omega$ : 1900 rpm,  $v$ : 10 mV s<sup>-1</sup>). The potential dependence of the number of electrons transferred per O<sub>2</sub> molecule calculated using the Koutecky–Levich equation from the corresponding RDE data (b, d and f).

the catalyst coated electrodes show higher ORR current density compared to the GC electrode. According to the ORR peak potential, the most positive value is always obtained in the case of GC/PDC-Co-N, which indicates that this catalyst is superior for the ORR compared to the other studied materials. However, the baseline current density seems to add a significant contribution to the LSV current density values. Therefore, the ORR was also studied under hydrodynamic conditions using the RDE method for more accurate evaluation of the ORR performance of the different catalyst materials.

**3.2.2 RDE studies of ORR and Koutecky–Levich analysis.** In Fig. 5a, c and e, the baseline-corrected RDE voltammetry curves of the catalysts recorded at 1900 rpm in solutions with different pH values are presented. Also, the RDE polarisation curves obtained with the commercial Pt/C catalyst are included for comparison purposes. Various parameters describing the ORR performance of the studied catalysts (*e.g.* onset potential ( $E_{\text{onset}}$ ), half-wave potential ( $E_{1/2}$ ), and  $\text{O}_2$  reduction current density at  $-0.2$  V) derived from the RDE polarisation curves are presented in Table S4.† According to these results, the commercial Pt/C catalyst is superior compared to all of the other non-noble metal catalysts studied in the present work. In the case of the PDC-based catalyst materials, the order of the ORR activity of the catalysts is similar to that observed in the case of LSVs in all the studied media. The pristine PDC material exhibited the lowest ORR performance, which could be explained by the absence of nitrogen and/or transition metal centres (see Fig. 4a) responsible for high ORR activity. After the catalysts were pyrolysed in the presence of DCDA, the  $E_{\text{onset}}$  and  $\text{O}_2$  reduction current density have remarkably improved due to the presence of nitrogen-containing groups (see Fig. 4b). A similar tendency has been observed in our previous works with different carbon-based catalysts before and after pyrolysis with DCDA.<sup>48,82,83</sup> Besides, the porous structure composed of mesopores, the increased pore sizes and specific surface areas of the N-doped materials suggest improved accessibility of active sites and lower mass-transfer limitations. Both the metal-doped catalyst coated electrodes (GC/PDC-Ni and GC/PDC-Co) exhibit higher ORR activity compared to the GC/PDC electrode indicating the positive impact of transition metals on the ORR performance, in line with previous observations.<sup>84</sup> Specifically, GC/PDC-Co shows better ORR activity than GC/PDC-Ni. A similar result has been obtained by Abdelwahab *et al.* in the case of Ni- and Co-doped carbon aerogels.<sup>85</sup> After pyrolysis of PDC-Ni in the presence of DCDA, the resulting catalyst material coated electrode (GC/PDC-Ni-N) shows a rather similar ORR activity to that of GC/PDC-N, but much lower ORR performance than the Co-containing catalyst. From that, we can assume that Ni does not form as many metal coordinated centres ( $\text{Me-N}_x$ ) during high-temperature pyrolysis or the ORR activity of Ni- $\text{N}_x$  is lower than that of its Co- $\text{N}_x$  counterpart. This is also supported by the study of Liu *et al.*,<sup>86</sup> where the influence of different metal dopants was explored in nitrogen-doped carbon xerogels: the  $E_{\text{onset}}$  value in 0.5 M  $\text{H}_2\text{SO}_4$  solution for the

Ni-doped and metal-free catalyst coated electrodes was very similar, while the Co-doped catalyst exhibited significantly higher electrocatalytic activity towards the ORR.<sup>86</sup>

Regarding the different media studied, a superior ORR performance was observed in alkaline media for all the materials. This result can be attributed to the change in active sites and their interaction with oxygen. This influence on ORR performance is supported by Wan *et al.*, where the effect of pH was studied on nitrogen-doped ordered mesoporous carbon.<sup>6</sup>

For the evaluation of the number of electrons ( $n$ ) transferred per  $\text{O}_2$  molecule from the RDE data of the different electrodes studied in the present work, the Koutecky–Levich (K-L) equation was used,<sup>87</sup>

$$\frac{1}{j} = \frac{1}{j_k} + \frac{1}{j_d} = -\frac{1}{nFkc_{\text{O}_2}^b} - \frac{1}{0.62nFD_{\text{O}_2}^{2/3}\nu^{-1/6}c_{\text{O}_2}^b\omega^{1/2}}$$

where  $j$  is the measured ORR current density at a specific potential  $E$ ,  $j_k$  and  $j_d$  are the kinetic and diffusion-limited current densities, respectively,  $k$  is the electrochemical rate constant for  $\text{O}_2$  reduction at a specific potential  $E$ ,  $F$  is the Faraday constant ( $96485 \text{ C mol}^{-1}$ ),  $\omega$  is the rotation rate of the electrode,  $c_{\text{O}_2}^b$  is the concentration of oxygen in the bulk ( $c_{\text{O}_2}^b$  in 0.5 M  $\text{H}_2\text{SO}_4$  is  $1.13 \times 10^{-6} \text{ mol cm}^{-3}$ ,<sup>88</sup> while in 0.1 M PBS and 0.1 M KOH it is  $1.2 \times 10^{-6} \text{ mol cm}^{-3}$ ),<sup>89</sup>  $D_{\text{O}_2}$  is the diffusion coefficient of oxygen ( $D_{\text{O}_2}$  in 0.1 M KOH is  $1.9 \times 10^{-5} \text{ cm}^2 \text{ s}^{-1}$ ,<sup>89</sup> while in 0.5 M  $\text{H}_2\text{SO}_4$  and 0.1 M PBS it is  $1.8 \times 10^{-5} \text{ cm}^2 \text{ s}^{-1}$ )<sup>88,90</sup> and  $\nu$  is the kinematic viscosity of the electrolyte solution ( $0.01 \text{ cm}^2 \text{ s}^{-1}$ ).<sup>91</sup>

The calculated  $n$  values for the different electrodes are presented in Fig. 5b, d and f. All the electrodes exhibit an  $n$  value between 2 and 4 in the studied potential ranges. As stated earlier, the 2-electron reduction corresponds to peroxide formation and the 4-electron process to the reduction of  $\text{O}_2$  to water.<sup>8,15</sup> Compared to the other electrodes, GC/PDC-Co-N indicates the highest  $n$  value in all the studied solutions. This is an expected result because the cobalt ion coordinated to nitrogen in the form of Co- $\text{N}_x$  (see section 3.1) plays an important role in the 4-electron reduction of  $\text{O}_2$ .<sup>45</sup> According to this, GC/PDC-Co-N is the most attractive ORR electrocatalyst for use at the low-temperature fuel cell cathode.

**3.2.3 The ORR activity of the PDC-Co-N catalyst.** Since the PDC-Co-N electrode exhibited the highest ORR activity compared to the other studied materials, the following discussion is therefore mainly focused on the PDC-Co-N catalyst. Fig. 6 depicts the RDE polarisation curves for  $\text{O}_2$  reduction in 0.1 M KOH at different rotation rates and the K-L plots derived from the corresponding RDE data on the GC/PDC-Co-N electrode. The diffusion-controlled  $\text{O}_2$  reduction is achieved at relatively low overpotentials as the K-L lines already coincide from *ca.* 0.4 V and the extrapolated K-L lines pass the origin of the axis. For comparison, the RDE polarisation curves at different electrode rotation rates and the corresponding K-L plots for GC/PDC-Co-N obtained in

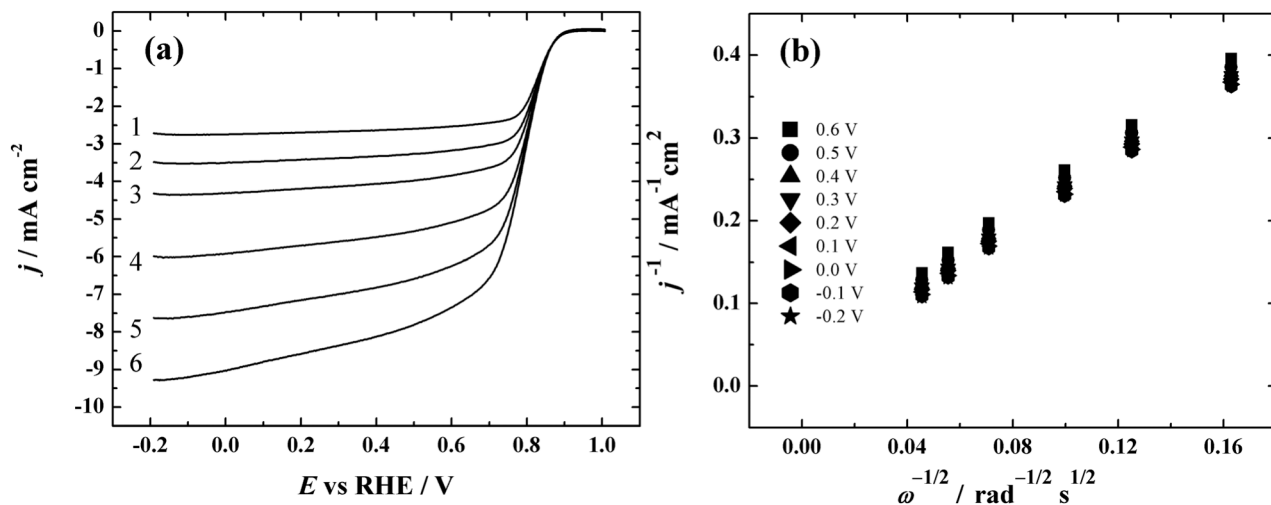


Fig. 6 RDE voltammetry curves for oxygen reduction on the GC/PDC-Co-N electrode in  $O_2$ -saturated 0.1 M KOH (pH = 13) ( $\omega$ : 1-360; 2-610; 3-960; 4-1900; 5-3100; 6-4600 rpm,  $\nu = 10 \text{ mV s}^{-1}$ ) (a), Koutecky–Levich plots for  $O_2$  reduction in 0.1 M KOH derived from the RDE data shown in Fig. 6a (b).

neutral and acidic media are shown in Fig. S7.† The current plateau of diffusion controlled  $O_2$  reduction is not as well developed as that in alkaline medium (Fig. 6a) and therefore, the extrapolated K-L lines pass the origin at relatively higher overpotentials compared to the RDE results obtained in 0.1 M KOH.

For potential application of PDC-Co-N as a fuel cell cathode catalyst, the long-term stability should be assessed. For this reason, an accelerated aging test was performed by cycling the catalyst coated electrode for 10 000 cycles between 0.6 and 1.0 V vs. RHE. The testing was carried out with GC/PDC-Co-N and Pt/C electrodes in alkaline solution and the obtained RDE polarisation curves are presented in Fig. 7. The  $E_{1/2}$  is about 34 mV more negative and the current density at 0.05 V has decreased by 6% after the potential cycling in the

case of the Pt/C electrode. Meanwhile, the corresponding values for GC/PDC-Co-N are 4 mV and less than 1%, respectively. These differences imply that the durability of the PDC-Co-N catalyst in an alkaline environment is remarkably higher compared to that of Pt/C.

There are a number of ORR studies describing Co-containing carbon based catalysts doped with nitrogen by pyrolysis. A comparison of the ORR performance with similar catalysts reported in the literature is presented in Table S5.† In the present work, an  $E_{\text{onset}}$  of 0.90 V and  $E_{1/2}$  of 0.80 V were determined for GC/PDC-Co-N in 0.1 M KOH at 1900 rpm (see Table S4†). For comparison, several more negative  $E_{\text{onset}}$  values have been reported for Co and nitrogen-containing catalysts in alkaline solution,<sup>22,46</sup> while very similar  $E_{\text{onset}}$  and  $E_{1/2}$  values were obtained in the case of Co-containing nitrogen-doped carbon aerogels in our earlier work.<sup>25</sup> Also, higher  $E_{\text{onset}}$  values can be found in some studies,<sup>36,38,45,47</sup> and the highest value has been obtained in the case of cobalt nanocrystals grown using nitrogen-doped graphene nanoparticles (1.06 V).<sup>28</sup> In neutral solutions,  $E_{\text{onset}}$  values of 0.59 V and 0.55 V (vs. RHE) have been reported for a NiCo-doped C-N nanocomposite in 0.5 M  $KNO_3$  (ref. 32) and for a square-like nano cobalt oxide anchored on N-doped graphene catalyst in PBS (pH = 7),<sup>27</sup> respectively. The latter catalyst was also studied for application in microbial fuel cells (MFCs).<sup>27</sup> In the present work, a considerably more positive value of 0.79 V (see Table S4 and Fig. 5c and S7a†) was obtained, which makes the PDC-Co-N catalyst also attractive for use under MFC conditions. In 0.5 M  $H_2SO_4$ , higher  $E_{\text{onset}}$  values than herein have been reported for materials pyrolysed with DCDA.<sup>20,47</sup> For example, Tang and Ng achieved a more positive  $E_{\text{onset}}$  value (0.90 V) for the Co- and N-codoped carbon catalyst prepared by pyrolysis of aniline and  $Co(NO_3)_2$  for MFC studies.<sup>34</sup> Nevertheless, considering previous information, the PDC-Co-N catalyst is comparable to the most active ORR catalysts of its type.

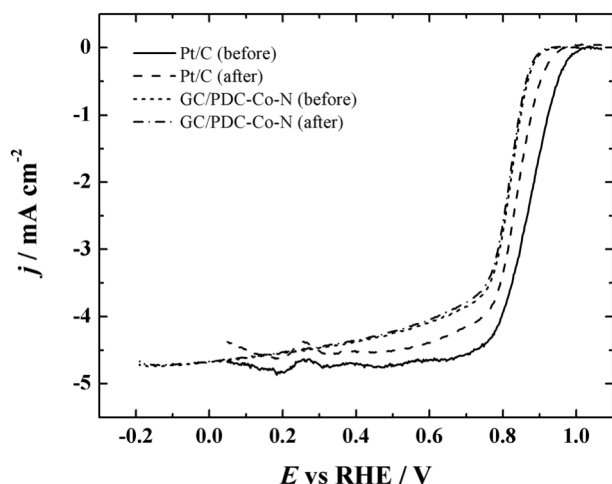


Fig. 7 RDE voltammetry curves for oxygen reduction on GC/PDC-Co-N and Pt/C catalysts in  $O_2$ -saturated 0.1 M KOH recorded before and after 10 000 cycles between 0.6 and 1 V in Ar-saturated 0.1 M KOH ( $\omega = 960 \text{ rpm}$ ,  $\nu = 10 \text{ mV s}^{-1}$ ).

Most of the electrocatalytic activity of the catalyst probably originates from the highly active Co-N<sub>x</sub> species;<sup>20,25,38,45–47</sup> their presence on PDC-Co-N was also supported by the XPS studies herein (see section 3.1). However, according to the XPS data, there is a considerably higher amount of N than Co in the PDC-Co-N catalyst (see Table S3†) and this refers to the presence of metal-free nitrogen functionalities. In papers describing Co-containing carbon-based ORR catalysts modified *via* pyrolysis with DCDA or other N precursors, one of the most active nitrogen species towards the ORR is proposed to be pyridinic-N.<sup>25,27,45,47,79</sup> The relevance of having pyridinic-N moieties is attributed to its nitrogen bonding with two carbons on the edge plane that gives rise to a structure with localized lone electron pairs and improved electron-donating ability.<sup>92</sup>

In the present study, the highest content of total nitrogen (see Table S3†) together with the highest relative content of pyridinic-N (see Table 1) was detected for PDC-Co-N amongst all the studied catalysts. In addition, the importance of pyridinic-N for the ORR has also been emphasised in studies regarding carbon-based Co- and N-codoped ORR catalysts for application in MFCs.<sup>27,34,93</sup> Besides, previous studies regarding Si-containing carbon materials have suggested that the presence of Si could improve the ORR activity, due to changes in the charge distribution and in the chemisorption mode of O<sub>2</sub>.<sup>94,95</sup> Also, the contribution to the enhanced ORR performance by the high surface area, confirmed by N<sub>2</sub> adsorption and CV experiments (see section 3.2.1), of the catalyst material must be considered.<sup>34,38</sup>

Considering all these findings, the PDC-Co-N material seems to be an active ORR electrocatalyst and therefore attractive for fuel cell applications.

## 4. Conclusions

Co/Ni-SiOC-based pristine and nitrogen doped electrocatalysts were proposed as a new class of catalysts for the ORR. The ORR kinetics was investigated in acid, neutral and alkaline media using the RDE technique. XPS and SEM-EDX results confirmed the successful N-doping of the PDC-based catalyst materials with DCDA. Both Co/Ni and nitrogen introduction to the PDC material exhibit positive effects on the ORR performance compared to the metal/nitrogen-free PDC-based materials. The Koutecky-Levich analysis yielded electron transfer numbers between 2 and 4, with the highest value for the PDC-Co-N catalyst. The results showed that PDC-Co-N catalyst possesses a superior electrocatalytic activity for the ORR compared to the other materials in all the studied media. The revealed performance is attributed to the higher amount of pyridinic-N and Co-N<sub>x</sub> centres. According to the stability testing results, the ORR performance of the PDC-Co-N catalyst remains almost unchanged after 10 000 CV cycles and its durability is superior as compared to the commercial Pt/C. Finally, this study provides the first findings of SiOC-based electrocatalysts to be considered in future material development as ORR catalysts for fuel cell technology.

## Conflicts of interest

There are no conflicts to declare.

## Acknowledgements

This work was financially supported by The Brazilian National Council for Scientific and Technological Development (CNPq) through the program Science without Borders within the process number 232484/2014-7. Additional support was provided by the Research Training Group GRK 1860 “Micro-, meso- and macroporous Nonmetallic Materials: Fundamental and Applications (MIMENIMA) and German Federal Ministry of Education and Research (BMBF) (INNO INDIGO project - 01DQ15013). The present work has been also financially supported by the Estonian Research Council (INNO INDIGO project) and institutional research funding (IUT20-16 and IUT2-24) of the Estonian Ministry of Education and Research. The EU has also supported this research through the European Regional Development Fund (TK141, “Advanced materials and high-technology devices for energy recuperation systems”). We would like to thank Dr. Jaan Aruväli for performing the XRD measurements at the University of Tartu.

## References

- O. Lori and L. Elbaz, *Catalysts*, 2015, 5, 1445–1464.
- K. Shimizu, L. Sepunaru and R. G. Compton, *Chem. Sci.*, 2016, 7, 3364–3369.
- H. Liu, R. Ramnarayanan and B. E. Logan, *Environ. Sci. Technol.*, 2004, 38, 2281–2285.
- M. Rahimnejad, A. Adhami, S. Darvari, A. Zirepour and S. E. Oh, *Alexandria Eng. J.*, 2015, 54, 745–756.
- S. Rojas-Carbonell, C. Santoro, A. Serov and P. Atanassov, *Electrochem. Commun.*, 2017, 75, 38–42.
- K. Wan, Z. P. Yu, X. H. Li, M. Y. Liu, G. Yang, J. H. Piao and Z. X. Liang, *ACS Catal.*, 2015, 5, 4325–4332.
- F. Zhao, F. Harnisch, U. Schröder, F. Scholz, P. Bogdanoff and I. Herrmann, *Environ. Sci. Technol.*, 2006, 40, 5193–5199.
- A. Sarapuu, E. Kibena-Pöldsepp, M. Borghei and K. Tammeveski, *J. Mater. Chem. A*, 2018, 6, 776–804.
- M. Shao, Q. Chang, J. P. Dodelet and R. Chenitz, *Chem. Rev.*, 2016, 116, 3594–3657.
- S. N. S. Goubert-Renaudin and A. Wieckowski, *J. Electroanal. Chem.*, 2011, 652, 44–51.
- C. Sealy, *Mater. Today*, 2008, 11, 65–68.
- L. M. Dai, Y. H. Xue, L. T. Qu, H. J. Choi and J. B. Baek, *Chem. Rev.*, 2015, 115, 4823–4892.
- F. Jaouen, E. Proietti, M. Lefevre, R. Chenitz, J. P. Dodelet, G. Wu, H. T. Chung, C. M. Johnston and P. Zelenay, *Energy Environ. Sci.*, 2011, 4, 114–130.
- G. Wu, A. Santandreu, W. Kellogg, S. Gupta, O. Ogoke, H. G. Zhang, H. L. Wang and L. M. Dai, *Nano Energy*, 2016, 29, 83–110.
- C. Song and J. Zhang, in *PEM Fuel Cell Electrocatalysts and Catalyst Layers: Fundamentals and Applications*, ed. J. Zhang, Springer, London, 2008, pp. 89–134.

- 16 Z. Y. Wu, Z. Iqbal and X. Q. Wang, *Front. Chem. Sci. Eng.*, 2015, 9, 280–294.
- 17 J. Lilloja, E. Kibena-Pöldsepp, M. Merisalu, P. Rauwel, L. Matisen, A. Niilisk, E. Cardoso, G. Maia, V. Sammelseg and K. Tammeveski, *Catalysts*, 2016, 6, 108.
- 18 M. Mooste, E. Kibena-Pöldsepp, L. Matisen, M. Merisalu, M. Kook, V. Kisand, V. Vassiljeva, A. Krumme, V. Sammelseg and K. Tammeveski, *Catal. Lett.*, 2018, 148, 1815–1826.
- 19 R. Li, X. Z. Wang, Y. F. Dong, X. Pan, X. G. Liu, Z. B. Zhao and J. S. Qiu, *Carbon*, 2018, 132, 580–588.
- 20 S. Ratso, I. Kruusenberg, A. Sarapuu, M. Kook, P. Rauwel, R. Saar, J. Aruväli and K. Tammeveski, *Electrochim. Acta*, 2016, 218, 303–310.
- 21 Z. L. Wang, S. Xiao, Z. L. Zhu, X. Long, X. L. Zheng, X. H. Lu and S. H. Yang, *ACS Appl. Mater. Interfaces*, 2015, 7, 4048–4055.
- 22 Y. C. Hao, Z. Y. Lu, G. X. Zhang, Z. Chang, L. Luo and X. M. Sun, *Energy Technol.*, 2017, 5, 1265–1271.
- 23 I. Kruusenberg, D. Ramani, S. Ratso, U. Joost, R. Saar, P. Rauwel, A. Kannan and K. Tammeveski, *ChemElectroChem*, 2016, 3, 1455–1465.
- 24 K. Kreek, A. Sarapuu, L. Samolberg, U. Joost, V. Mikli, M. Koel and K. Tammeveski, *ChemElectroChem*, 2015, 2, 2079–2088.
- 25 A. Sarapuu, L. Samolberg, K. Kreek, M. Koel, L. Matisen and K. Tammeveski, *J. Electroanal. Chem.*, 2015, 746, 9–17.
- 26 K. Kisand, A. Sarapuu, A. Peikolainen, H. Seemen, M. Kook, M. Käärrik, J. Leis, V. Sammelseg and K. Tammeveski, *ChemElectroChem*, 2018, 5, 2002–2009.
- 27 C. Cao, L. L. Wei, M. Su, G. Wang and J. Q. Shen, *RSC Adv.*, 2016, 6, 52556–52563.
- 28 L. B. Lv, T. N. Ye, L. H. Gong, K. X. Wang, J. Su, X. H. Li and J. S. Chen, *Chem. Mater.*, 2015, 27, 544–549.
- 29 X. Wan, H. J. Wang, H. Yu and F. Peng, *J. Power Sources*, 2017, 346, 80–88.
- 30 Q. J. Mo, N. N. Chen, M. D. Deng, L. C. Yang and Q. S. Gao, *ACS Appl. Mater. Interfaces*, 2017, 9, 37721–37730.
- 31 K.-K. Türk, I. Kruusenberg, J. Mondal, P. Rauwel, J. Kozlova, L. Matisen, V. Sammelseg and K. Tammeveski, *J. Electroanal. Chem.*, 2015, 756, 69–76.
- 32 Z. Deng, Q. Yi, G. Li, Y. Chen, X. Yang and H. Nie, *Electrochim. Acta*, 2018, 279, 1–9.
- 33 F. Guo, H. Yang, B. Aguila, A. M. Al-Enizi, A. Nafady, M. Singh, V. Bansal and S. Q. Ma, *Catal. Sci. Technol.*, 2018, 8, 5244–5250.
- 34 X. H. Tang and H. Y. Ng, *Electrochim. Acta*, 2017, 247, 193–199.
- 35 G. M. Kim, S. Baik and J. W. Lee, *RSC Adv.*, 2015, 5, 87971–87980.
- 36 S. Ratso, I. Kruusenberg, M. Käärrik, M. Kook, L. Puust, R. Saar, J. Leis and K. Tammeveski, *J. Power Sources*, 2018, 375, 233–243.
- 37 A. Q. Zhu, P. F. Tan, L. Qiao, Y. J. Liu, Y. Ma, X. Xiong and J. Pan, *Inorg. Chem. Front.*, 2017, 4, 1748–1756.
- 38 T. T. Sun, L. B. Xu, S. Y. Li, W. X. Chai, Y. Huang, Y. S. Yan and J. F. Chen, *Appl. Catal., B*, 2016, 193, 1–8.
- 39 Q. Q. Cheng, L. J. Yang, L. L. Zou, Z. Q. Zou, C. Chen, Z. Hu and H. Yang, *ACS Catal.*, 2017, 7, 6864–6871.
- 40 J. J. Yan, H. Y. Lu, Y. P. Huang, J. Fu, S. Y. Mo, C. Wei, Y. E. Miao and T. X. Liu, *J. Mater. Chem. A*, 2015, 3, 23299–23306.
- 41 C. Liu, J. Wang, J. S. Li, J. Z. Liu, C. H. Wang, X. Y. Sun, J. Y. Shen, W. Q. Han and L. J. Wang, *J. Mater. Chem. A*, 2017, 5, 1211–1220.
- 42 K. X. Liu, S. Kattel, V. Mao and G. F. Wang, *J. Phys. Chem. C*, 2016, 120, 1586–1596.
- 43 J. P. McClure, R. Z. Jiang, D. Chu and P. S. Fedkiw, *Carbon*, 2014, 79, 457–469.
- 44 S. Bhattacharyya, B. Konkena, K. Jayaramulu, W. Schuhmann and T. K. Maji, *J. Mater. Chem. A*, 2017, 5, 13573–13580.
- 45 R. Zhang, L. Liu, J. Zhang, W. Y. Wang, F. Ma, R. F. Li and L. Z. Gao, *J. Solid State Electrochem.*, 2015, 19, 1695–1707.
- 46 Y. D. Qian, Z. Liu, H. Zhang, P. Wu and C. X. Cai, *ACS Appl. Mater. Interfaces*, 2016, 8, 32875–32886.
- 47 Q. P. Zhao, Q. Ma, F. P. Pan, J. H. Guo and J. Y. Zhang, *Ionics*, 2016, 22, 2203–2212.
- 48 S. Ratso, I. Kruusenberg, M. Käärrik, M. Kook, R. Saar, M. Pärs, J. Leis and K. Tammeveski, *Carbon*, 2017, 113, 159–169.
- 49 R. L. McCreery, *Chem. Rev.*, 2008, 108, 2646–2687.
- 50 R. Borup, J. Meyers, B. Pivovar, Y. S. Kim, R. Mukundan, N. Garland, D. Myers, M. Wilson, F. Garzon, D. Wood, P. Zelenay, K. More, K. Stroh, T. Zawodzinski, J. Boncella, J. E. McGrath, M. Inaba, K. Miyatake, M. Hori, K. Ota, Z. Ogumi, S. Miyata, A. Nishikata, Z. Siroma, Y. Uchimoto, K. Yasuda, K. I. Kimijima and N. Iwashita, *Chem. Rev.*, 2007, 107, 3904–3951.
- 51 L. David, R. Bhandavat, U. Barrera and G. Singh, *Nat. Commun.*, 2016, 7, 10998.
- 52 M. S. Kolathodi, L. David, M. A. Abass and G. Singh, *RSC Adv.*, 2016, 6, 74323–74331.
- 53 P. Greil, *J. Am. Ceram. Soc.*, 1995, 78, 835–848.
- 54 M. Adam, M. Wilhelm and G. Grathwohl, *Microporous Mesoporous Mater.*, 2012, 151, 195–200.
- 55 P. Greil, *J. Eur. Ceram. Soc.*, 1998, 18, 1905–1914.
- 56 M. Scheffler, P. Greil, A. Berger, E. Pippel and J. Woltersdorf, *Mater. Chem. Phys.*, 2004, 84, 131–139.
- 57 C. Vakifahmetoglu, E. Pippel, J. Woltersdorf and P. Colombo, *J. Am. Ceram. Soc.*, 2010, 93, 959–968.
- 58 C. Harms, M. Adam, K. A. Soliman, M. Wilhelm, L. A. Kibler, T. Jacob and G. Grathwohl, *Electrocatalysis*, 2014, 5, 301–309.
- 59 M. Wojcik-Bania, A. Krowiak, J. Strzezik and M. Hasik, *Mater. Des.*, 2016, 96, 171–179.
- 60 M. Schubert, M. Wilhelm, S. Bragulla, C. H. Sun, S. Neumann, T. M. Gesing, P. Pfeifer, K. Rezwan and M. Bäumer, *Catal. Lett.*, 2017, 147, 472–482.
- 61 V. L. Nguyen, N. B. Laidani and G. D. Soraru, *J. Mater. Res.*, 2015, 30, 770–781.
- 62 J. F. Drillet, M. Adam, S. Barg, A. Herter, D. Koch, V. M. Schmidt and M. Wilhelm, *ECS Trans.*, 2010, 28, 13–24.

- 63 F. Schlüter, J. Meyer, M. Wilhelm and K. Rezwan, *Colloids Surf., A*, 2016, **492**, 160–169.
- 64 S. Kabir, K. Artyushkova, A. Serov, B. Kiefer and P. Atanassov, *Surf. Interface Anal.*, 2016, **48**, 293–300.
- 65 K. Artyushkova, I. Matanovic, B. Halevi and P. Atanassov, *J. Phys. Chem. C*, 2017, **121**, 2836–2843.
- 66 P. Moni, M. Wilhelm and K. Rezwan, *RSC Adv.*, 2017, **7**, 37559–37567.
- 67 IUPAC, *Manual of Symbols and Terminology for Physicochemical Quantities and Units*, London Butterworths, Bristol, UK, 1972.
- 68 Z. A. Alothman, *Materials*, 2012, **5**, 2874–2902.
- 69 M. Kruk and M. Jaroniec, *Chem. Mater.*, 2001, **13**, 3169–3183.
- 70 M. Wilhelm, M. Adam, M. Bäumer and G. Grathwohl, *Adv. Eng. Mater.*, 2008, **10**, 241–245.
- 71 P. Colombo, G. Mera, R. Riedel and G. D. Soraru, *J. Am. Ceram. Soc.*, 2010, **93**, 1805–1837.
- 72 G. Zhao, T. S. Zhao, J. Xu, Z. Lin and X. Yan, *Int. J. Hydrogen Energy*, 2017, **42**, 3325–3334.
- 73 X. D. Zhang, X. X. Huang, G. W. Wen, X. Geng, J. D. Zhu, T. Zhang and H. W. Bai, *Nanotechnology*, 2010, **21**, 385601.
- 74 Z. Q. Luo, S. H. Lim, Z. Q. Tian, J. Z. Shang, L. F. Lai, B. MacDonald, C. Fu, Z. X. Shen, T. Yu and J. Y. Lin, *J. Mater. Chem.*, 2011, **21**, 8038–8044.
- 75 D. M. K. Abro, P. Dablé, F. Cortés-Salazar, V. Amstutz and H. Girault, *J. Miner. Mater. Charact. Eng.*, 2016, **4**, 62.
- 76 S. Roualdes, R. Berjoan and J. Durand, *Sep. Purif. Technol.*, 2001, **25**, 391–397.
- 77 K. Yamamoto, Y. Koga and S. Fujiwara, *Diamond Relat. Mater.*, 2001, **10**, 1921–1926.
- 78 S. H. Gage, D. A. Ruddy, S. Pylypenko and R. M. Richards, *Catal. Today*, 2018, **306**, 9–15.
- 79 H. S. Oh and H. Kim, *J. Power Sources*, 2012, **212**, 220–225.
- 80 M. Mooste, E. Kibena-Pöldsepp, L. Matisen and K. Tammeveski, *Electroanalysis*, 2017, **29**, 548–558.
- 81 M. Mooste, E. Kibena-Pöldsepp, B. D. Ossoinon, D. Bélanger and K. Tammeveski, *Electrochim. Acta*, 2018, **267**, 246–254.
- 82 M. Vikkisk, I. Kruusenberg, U. Joost, E. Shulga, I. Kink and K. Tammeveski, *Appl. Catal., B*, 2014, **147**, 369–376.
- 83 R. Sibul, E. Kibena-Pöldsepp, S. Ratso, M. Kook, M. Käärik, M. Merisalu, P. Paiste, J. Leis, V. Sammelseg and K. Tammeveski, *Electrochem. Commun.*, 2018, **93**, 39–43.
- 84 N. Gavrilov, M. Momcilovic, A. S. Dobrota, D. M. Stankovic, B. Jokic, B. Babic, N. V. Skorodumova, S. V. Mentus and I. A. Pasti, *Surf. Coat. Technol.*, 2018, **349**, 511–521.
- 85 A. Abdelwahab, J. Castelo-Quibén, J. Vivo-Vilches, M. Pérez-Cadenas, F. Maldonado-Hódar, F. Carrasco-Marín and A. Pérez-Cadenas, *Nanomaterials*, 2018, **8**, 266.
- 86 S. S. Liu, C. W. Deng, L. Yao, H. X. Zhong and H. M. Zhang, *J. Power Sources*, 2014, **269**, 225–235.
- 87 A. J. Bard and L. R. Faulkner, *Electrochemical Methods: Fundamentals and Applications*, Wiley, New York, 2nd edn, 2001.
- 88 S. Gottesfeld, I. D. Raistrick and S. Srinivasan, *J. Electrochem. Soc.*, 1987, **134**, 1455–1462.
- 89 R. E. Davis, G. L. Horvath and C. W. Tobias, *Electrochim. Acta*, 1967, **12**, 287–297.
- 90 F. King, C. D. Litke and Y. Tang, *J. Electroanal. Chem.*, 1995, **384**, 105–113.
- 91 D. R. Lide, *CRC Handbook of Chemistry and Physics*, CRC Press, Boca Raton, 82nd edn, 2001.
- 92 G. Liu, X. G. Li, P. Ganesan and B. N. Popov, *Appl. Catal., B*, 2009, **93**, 156–165.
- 93 K. K. Türk, I. Kruusenberg, E. Kibena-Pöldsepp, G. D. Bhowmick, M. Kook, K. Tammeveski, L. Matisen, M. Merisalu, V. Sammelseg, M. M. Ghangrekar, A. Mitra and R. Banerjee, *Int. J. Hydrogen Energy*, 2018, **43**, 23027–23035.
- 94 Z. Liu, X. Fu, M. Li, F. Wang, Q. Wang, G. Kang and F. Peng, *J. Mater. Chem. A*, 2015, **3**, 3289–3293.
- 95 S. C. Abbas, K. Ding, Q. Liu, Y. Huang, Y. Bu, J. Wu, J. Lv, M. A. Ghausi and Y. Wang, *J. Mater. Chem. A*, 2016, **4**, 7924–7929.